Drift Chamber Experiment

A.H. Walenta, T. Çonka Nurdan, and K. Nurdan
University of Siegen, FB Physik, ENC Walter-Flex-Str. 3 57072 Siegen, Germany

S. Özkorucuklu
Süleyman Demirel University, Physics Department, Çünür Kampüsü, 32260 Isparta, Turkey

This paper describes a laboratory course held at 2nd Local ICFA Instrumentation School at the ICFA Center Istanbul. This course intends to introduce drift chambers, which play an important role in particle physics experiments as tracking detectors. The experimental setup consists of a single-sided, single-cell drift chamber, a plastic scintillator detector and a collimated ^{90}Sr source. The measurements on the drift velocity of electrons, its change as a function of a drift field, gas gain and diffusion are performed at this laboratory course.

INTRODUCTION

Drift chambers play a major role in particle physics experiments as detectors for tracking of charged particles for a number of reasons:

- construction of large detectors (4m x 4m)
- high precision (typically $\sigma = 100$ μm)
- 2D position measurement
- operation in magnetic field (with some precaution)
- particle identification
- simple construction in standard machine shops / laboratories
- economic read-out

The basic principle of operation makes use of the fact that the timing of the signal in a proportional counter shows a time lag with respect to the moment of particle passage (and consequently the moment of creation of the ionization along the particle track in the gas of the detector volume). This time lag is related to the time the electrons from the ionization take to travel (drift) to the amplifying anode wire (fig. 1). In proportional counters this time lag is considered as a nuisance limiting the time resolution of the detector. If, however, the timing of the particle passage is determined with higher precision by scintillating counters (hodoscopes) or by the timing of the accelerator bunch, the time lag can be used to determine the exact position of the ionization with respect to the anode wire. It is clear that the quality of the relation drift time vs. drift distance determines the quality of the position measurement.

Mathematically the measured drift time t_{drift} is related to the drift path (for zero magnetic field along the electrical field lines) from the location of ionization creation along the track to the anode by:

$$t_{drift} = \int_{track}^{anode} \frac{ds}{v(\vec{x})} \tag{1}$$

For operational devices two basic schemes have been conceived: the method of constant drift field (fig. 2a) giving a simple dependence for the drift distance $d = t_{drift} \cdot v_{drift}$ with v_{drift} = constant and the second method with variable drift field (mostly radial dependence as in a cylindrical geometry of a proportional counter tube) where the gas is chosen such that the drift velocity is independent or only slightly dependent on the drift field. For the latter a calibration procedure is applied determining the closest approach of the track s_{min} to the anode (fig. 2b). In order to cover larger surfaces these cells have to be repeated which requires in addition a solution for the right-left ambiguity. This can be achieved by the "double wire method" (fig. 3a) or by the "staggering method" (fig. 3b). Other structures used in volume detectors for cylindrical trackers for colliding beam experiments are the jet chamber (fig. 4(a)) and the somewhat particular geometry introduced by the so called Time Projection Chamber (TPC, fig. 4(b)), where in a cylindrical geometry the full 3 dimensional track drifts towards the detector plane at the end cap and is recorded in

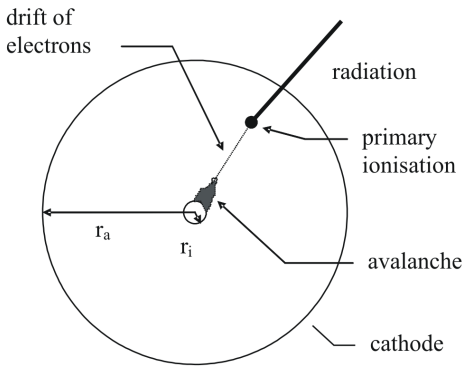

FIG. 1: *Principle of proportional counter*

two spatial and one timing coordinates (hence the name). This geometry has the advantage of full 3D reconstruction with a relatively small number of read out channels as compared to the number of resolved volume elements such that an amplitude measurement can be implemented yielding information about the ionization loss. This additional information can be used for particle identification.

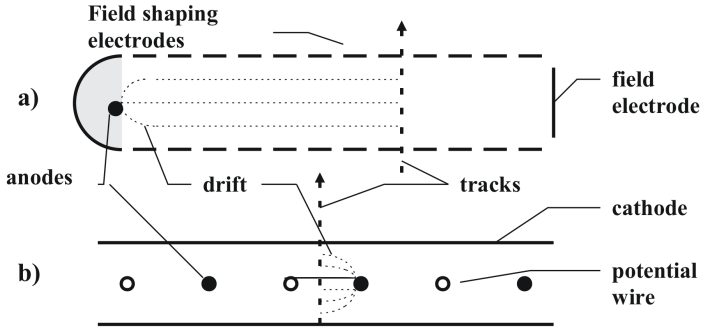

FIG. 2: *Principle of drift chambers. a) constant drift field b) multi wire drift chamber*

Theoretical Background

Ionization By Charged Particles

In fig. 2 the track of the charged particle is indicated as a dashed line, which may be interpreted as the path of the projectile. This is a rather abstract representation of the reality consisting of an accumulation of ionization clusters (fig. 5).

The ionization clusters are produced in the following way: the time dependent electrical field of the passing particle couples to the electrons of the gas atoms and may have enough impact to kick out the electron of an atomic shell, say the L-shell, causing an energy transfer E′. The excess energy E_{Kin}= E′- E_L represents the kinetic energy of this liberated electron which in turn may ionize again. In this case it considered as a new charged particle and is called δ-ray. If the excess energy is low it will not ionize and thermalize quickly. The ionization left behind by these individual encounters, including the rearrangement of the L-shell, mediated by Auger-electrons or x-ray emission, is called a cluster and the sum of the clusters represents the footprint of the charged particle, which will be detected in the drift chamber. Therefore it is important to know some features:

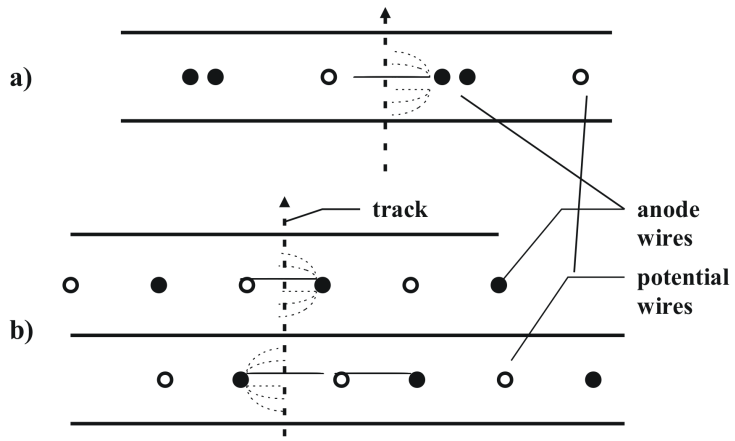

FIG. 3: *Right-left ambiguity in drift chambers. a) double wire type b) double chamber type*

1. the number of the clusters per track length
2. the spatial distribution along the track
3. their size, measured in terms of the number of free electrons belonging to them
4. their spatial extension

If Φ (E′, E) dE′dx is the probability for an energy loss in the interval between E′ and E′+ dE′ of the charged particle with energy E along a track segment dx the number of such encounters per track length is given by

$$\langle \frac{dN}{dx} \rangle = \int_{E'_{\min}}^{E'_{\max}} \Phi(E', E) dE' \tag{2}$$

where the integration extends from the smallest possible energy transfer E'_{min} to the largest E'_{max}. Since Φ (E′, E) also contains encounters leading to excitation of the atom the number of ionization clusters is obtained if only those encounters are considered leading to ionization.
A good approximation can be obtained from a simple collision model (Bohr's model):

$$\Phi(E', E) dE' dx = \frac{\tilde{A}\rho}{\beta^2} \frac{1}{E'^2} dE' dx \tag{3}$$

with ρ the gas density, β=v/c, and Ã=0.1536 Z/A MeV cm^2 g^{-1}. Inserting (3) into (2) yields:

$$\langle \frac{dN}{dx} \rangle = \frac{\tilde{A}\rho}{\beta^2} \left(\frac{1}{E'_{\min}} - \frac{1}{E'_{\max}} \right) \approx \frac{\tilde{A}\rho}{\beta^2} \frac{1}{E'_{\min}} \tag{4}$$

which takes into account $E'_{max} >> E'_{min}$. For the calculation of E'_{min} the quantum mechanical effects cannot be neglected and therefore a simple formula has not been developed. For a few gases numerical values have been obtained, either calculated from approximative shell models or measured in cloud chambers, streamer chambers, proportional counters and drift chambers. A selection is given in table I where the columns belong to a set with a given speed of the projectile characterized by $\gamma = \sqrt{1/(1\text{-}\beta^2)}$. The minimum of ionization is found at $\gamma \cong$ 3,2..3,5 while at $\gamma \cong 4$ the relativistic rise is noticeable.

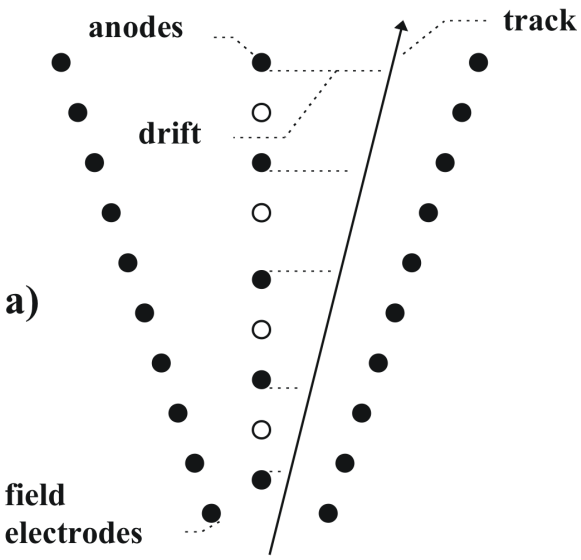

(a) *Drift chamber for storage ring experiments. Jet chamber section*

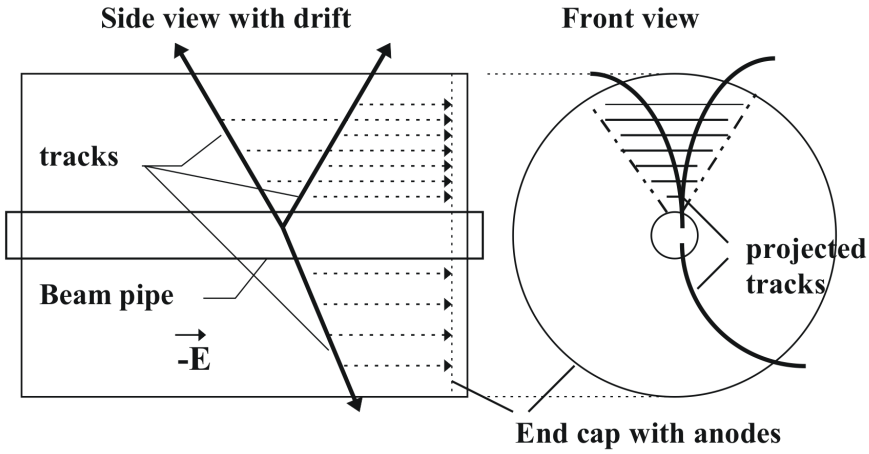

(b) *Drift chamber for storage ring experiments in a magnetic field. Time projection chamber (TPC)*

FIG. 4: *Drift chambers for storage ring experiments*

TABLE 1. Gases for proportional counters and drift chambers.

Gas	**A,M**	ρ **(mg/cm^3)**	$\tilde{\mathbf{A}}$ **(keV/cm)**	$\mathbf{n_p/cm}$ γ**=3,2...3,5 a)**	$\mathbf{n_p/cm}$ γ**=4,0 b)**	$\mathbf{n_p/cm}$ γ**=4,0 calc c)**	$\mathbf{n_p/cm}$ γ**=min d)**	$\mathbf{n_p/cm}$ $\gamma\cong$**min prop. e)**
He	4,0	0,166	0,0127	3,83	5,02	3,6	4,64	
Ne	20,18	0,839	0,0644	11,6	12,4	12,7	10,84	
Ar	39,95	1,66	0,115	28,6	27,8	29,3	22,6	
Kr	83,8	3,45	0,227			35,4		

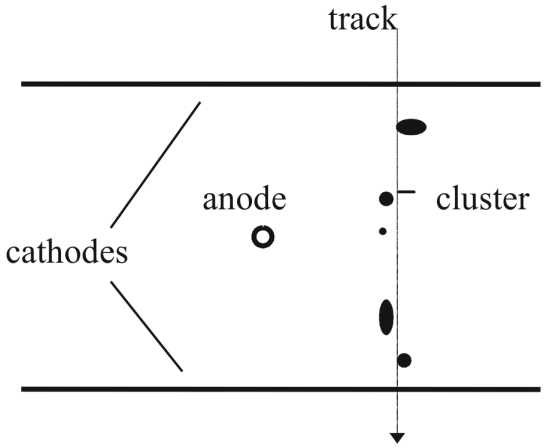

FIG. 5: *Ionization cluster distribution along track (schematically)*

Xe	131,3	5,40	0,342		44	48,1	42,60	
H_2	2,0	0,0838	0,0137	4,55	5,32	5,1	4,72	
N_2	28,0	1,165	0,096			22,3		
O_2	32,0	1,331			22,2	26,6		
Air	28,9	1,204	0,099	18,5		25,4	23,1	
C_2H_6	30,02	1,26	0,116				40,7	
C_3H_8	44,03	1,87	0,171				68,8	
C_4H_{10}	58,04	2,52	0,227				87,1	41,8
P-10	36,75	1,5608	0,109					13,4
CO_2	44,0	1,84	0,140				33,2	
Ne, CH_4			0,077					13,7
0,5 Ar, 0,5 C_4H_{10}			0,15					26,2

Measured and calculated values do not agree very well but the general dependence of equ. (4) is reproduced (fig. 6). For a set of measurements or calculations a value of E′ = 2.8 eV and 6,2 eV is found within the expectation.

Since the generation of an individual ionization cluster is completely random the actual number in a chamber m_p varies according to a Poisson distribution. This is responsible as well for the random distribution along the track resulting in an exponential probability distribution of the gaps between two clusters.

The cluster size distribution is governed by the energy loss distribution described by Φ (E′, E) such that the number of electrons is typically E′/W with W the energy necessary to create an ion pair. Following the steep decrease of Φ (E′, E) most of the clusters will be single electron clusters and larger clusters will occur only occasionally. These large clusters can be considered as small tracks on their own (δ-rays) and their range is responsible for the spatial extension of the clusters, which may reach a few hundred microns in a counting gas at NTP.

In a similar way as the mean number of clusters in equ. (2) the mean energy loss for a track segment is obtained by

$$\langle \frac{dE}{dx} \rangle = \int_{E'_{\min}}^{E'_{\max}} E' \Phi(E', E) dE' \tag{5}$$

which is called the mean energy loss. Taking into account relativistic effects and relation (3) the well-known Bethe-Bloch formula is obtained:

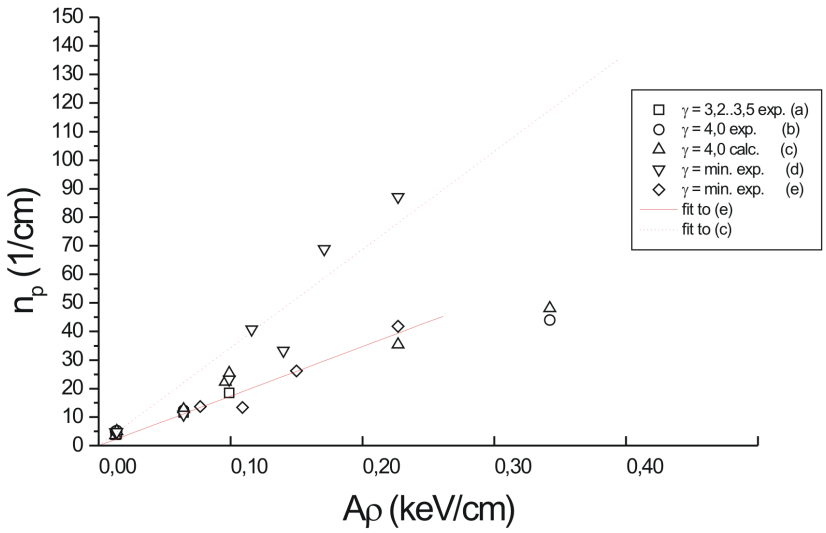

FIG. 6: *Mean number of primary clusters in different gases*

$$\langle \frac{dN}{dx} \rangle = \frac{\tilde{A}\rho}{\beta^2}(2\ln\frac{2m_e c^2}{\bar{I}^2} + 2\ln\beta\gamma - 2\beta^2 - 2\delta) \tag{6}$$

where $\bar{I}$ is the mean ionization potential and δ the density correction. The fluctuations of the energy loss are given by an asymmetric rather broad Landau distribution with a long tail towards higher energy. A good description of this distribution is obtained using the most probable energy loss E_{mp} and the full width at half maximum ΔE. The properties of this distribution become important in the light of a possible application for particle identification using either the $1/\beta^2$ dependence in the non relativistic case or the logarithmic rise in the relativistic part of the energy loss (equ. (6)). Since the fluctuations of the Landau distribution are rather large ($\Delta E/E_{mp}$ = 0,40... 1,0) only a method of multiple sampling yields the necessary resolution of about 6%.

The Proportional Gas Gain

Originally the proportional counter is used in a cylindrical geometry, i.e. a wire with a radius r_i of less than 50 μm is stretched in the center of a tube (outer cylinder) with a radius r_a of typically a centimeter (see fig. 1).

The inner wire is held at positive potential U_0 with respect to the outer cylinder resulting in the known potential U(r) and field distribution E(r) of a cylindrical capacitor:

$$E(r) = \frac{U_0}{r}\frac{1}{\ln\frac{r_i}{r_a}} \tag{7}$$

$$U(r) = \frac{U_0}{\ln\frac{r_i}{r_a}}\ln\frac{r}{r_a} \tag{8}$$

The sealed tube is filled with a counting gas adapted to the desired performance of the detector. For most applications an Argon mixture is sufficient (P-10: 0.9 Ar + 0.1 CH_4) which exhibits excellent counting performance. A quencher gas (e.g. CH_4, CO_2) is added in order to obtain lower diffusion of the drifting electrons and in order to control the gas gain. For the efficient absorption of x- and γ- rays a dense gas with high atomic number (Xe) is used. The latter takes place in the vicinity of the anode wire where the field strength becomes large enough to generate

an avalanche. Each primary electron contributes to the total charge in the avalanche G ion pairs where G is called gas amplification. Using the assumption that the gas multiplication is only due to the accelerated electrons ionizing the gas atoms then the growth of the avalanche dn on the path length dr is described by the Townsend process dn = α·n·dr with the Townsend coefficient α and consequently for the total avalanche the gain G is calculated:

$$\ln G = -\int_{r_1}^{r^2} \alpha(r)dr = \int_{r_i}^{r_a} \alpha(r)dr \tag{9}$$

The integration extends from the threshold radius r_1 to the surface of the anode wire $r_2 = r_i$. For simplicity the integration can be carried out from the outer (cathode) radius $r_a = r_k$ since the additional contribution will vanish. The Townsend coefficient α is a function of the electrical field strength and therefore it becomes a function of r as well.

In practice the evaluation of the integral fails because of the limited knowledge of α. Mostly simple (linearized) approximations are used resulting in formulas for the gas gain of limited use. A more satisfactory parameterization of α is obtained in the form

$$\frac{\alpha}{p} = A\exp(-B(p/E)^k) \tag{10}$$

with A, B and k experimental parameters.

It was found that k=0.65 describes well measurements with noble gas - hydrocarbon mixtures (Ar/CH_4) and pure hydrocarbon [9]. Under this assumption the formula contains only two experimental parameters.

This parameterization still leads to a complicated integral but numerical integration is straightforward. Table 2 gives the parameters used for several gases and mixtures.

TABLE 2.

Gas	**A (1/Torr mm)**	**B (kV/Torr mm)ˆk**	**k**
P-10 (0.9 Ar/0.1 CH_4)	1.844	0.1044	0.65
Ar	1.40	0.018	1.0
Iso-butane, C_4H_{10}	6.748	0.24064	0.65
Xe/CO_2 (0.95/0.05)	2.60	0.125	0.65
Xe	2.60	0.035	1.0
H_2	0.5	0.013	1.0
CO_2	2.0	0.0466	1.0
N_2	1.2	0.0342	1.0

Fig.7 shows the values for α/p as function of the reduced field calculated with the parameters given in Table II. The parameter A defines the plateau, which is related to the maximum cross section for ionization by electron impact. The parameter B defines the onset of the rise and is related to the energy distribution of the electrons in the swarm and therefore is influenced by the inelastic cross section of electron scattering. Small admixtures of molecular gases have a strong influence. The parameter k changes the slope in the steeply rising section. Since the gas gain takes place in the field region E/p= 10^{-3} to 10^{-2} kV/mm Torr the most important parameter is B which is responsible for the high voltage needed for sufficient gas gain. This can be seen in fig. 8 where the gases with large B follow this rule.

The gas gain obtained for P-10 and isobutane (fig. 8) shows also the effect of the anode wire dimensions from r_i = (7.5 μm and 15 μm) in comparison with the measurements [9].

In summary it can be stated that the integration of the Townsend coefficient parameterized in the given form reproduces well the observed gas amplification in proportional counters. Clearly the extreme effects caused by different discharge phenomena are not described as limited proportional or streamer mode where the propagation and ionization of uv-quanta plays an important role. In these cases the second Townsend coefficient has to be taken into account. Here we are limited to the pure proportional mode.

Drift And Diffusion

As relation (1) indicates the drift velocity of electrons in gases as a function of the electric field is of foremost importance for the proper operation of a drift chamber. The basic process of the motion of free electrons in gases

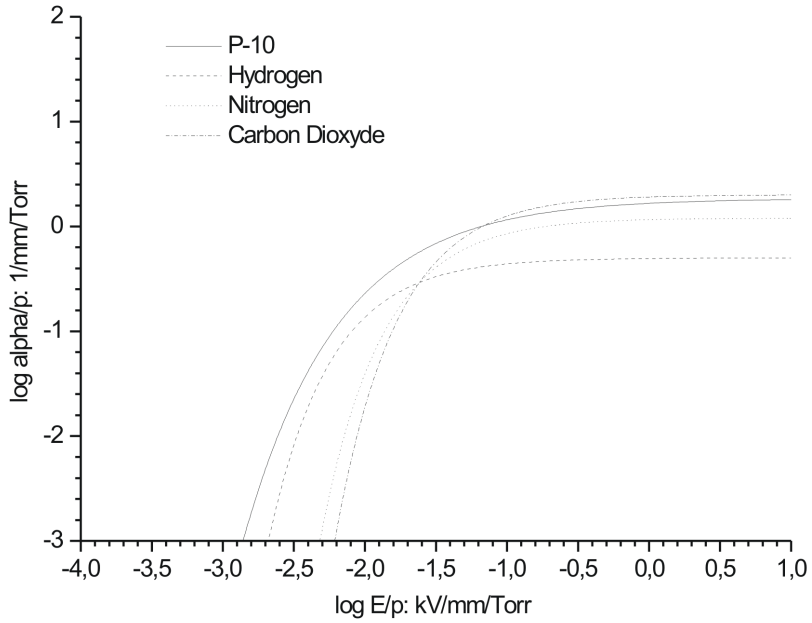

FIG. 7: *Townsend coefficient for few selected gases*

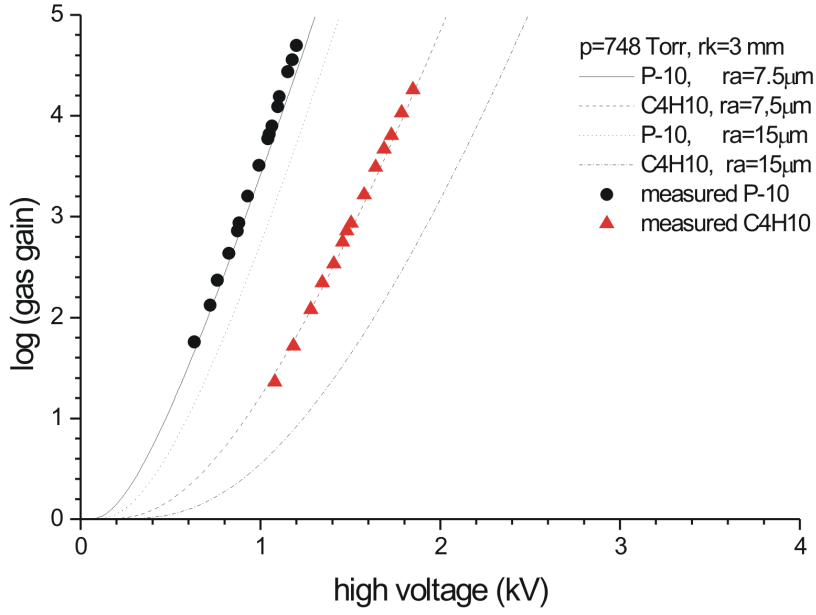

FIG. 8: *Gas gain calculated and measured*

is described by the diffusion of thermalized electrons superimposed by a directional motion of drift under the force created by the electrical field acting on the charge of the electrons. In a "mean electron model" (where the Maxwell -like energy distribution of the electrons is replaced by an appropriate mean energy ε or the mean velocity c = $\sqrt{8/3\pi}$ · $\sqrt{2\varepsilon/\mathrm{m}}$) the diffusion is described by a broadening of an initial delta function for the spatial distribution into a gaussian distribution with

$$\sigma = \sqrt{2Dt} \tag{11}$$

where the diffusion coefficient is given by

$$D = \frac{1}{3}c\lambda \tag{12}$$

The drift velocity in this model is given by

$$V_{drift} = \frac{8}{3\pi}\frac{e}{m}\frac{E}{c}\lambda = \mu \cdot E \tag{13}$$

with μ the mobility and E the electrical field strength. It is seen that the mean free path λ (and consequently the cross section for electron scattering at the atoms) as a function of the mean electron energy and the mean electron energy as a function of the reduced electric field E/p determine the motion parameters v_{drift} and D.

In the usual drift gases a mixture of a noble gas (mostly Ar) with a molecular admixture (mostly hydro-carbons like C_n H_m) are used. In order to emphasize the atomic and molecular physics, the mobility μ is considered: with increasing field E the electrons are accelerated but the velocity c is increasing only to a limit since the onset of inelastic cross sections (rotational and excitational processes) absorb most of the energy from the field. However, the small change in c reduces the total cross section considerably due to the Ramsauer effect, where atoms become transparent to the electrons. Therefore the mobility rises sharply for small fields. At somewhat higher fields and energies the rotational cross sections become constant, therefore c rises quickly reducing the mobility. In concert with the increase of the cross section behind the Ramsauer minimum, the mobility may even drop to an extent that the drift velocity is dropping as well. This effect can be seen very well in the standard P-10 mixture (90% Ar, 10% CH_4). Clearly, the proper choice of the gas mixture allows over a wide range of E to obtain an almost constant drift velocity (see fig. 9), which is important for a good position resolution and a stable operation.

In order to obtain some insight to the diffusion process it is useful to consider the following relation (Einstein relation):

$$e\frac{D}{\mu} = kT_e \tag{14}$$

where e is the electron charge and T_e the electron temperature that coincides with the gas temperature if the "heating" of the electrons by the electric field is negligible. For gases with large inelastic cross section for electron collisions this will be the case even for large electric field strength (cool gases). For noble gases or noble gas mixtures with a small admixture of molecular gases (e.g. P-10) the deviation starts already at small drift field. This is best seen in fig. 10 by the relation obtained for the experimentally accessible quantity σ, as function of E and l (the drift length) by combining equ. 1,2,4,5:

$$\frac{\sigma^2}{l} = \frac{2}{e}\frac{kT}{E} \tag{15}$$

The measured quantity σ^2/l representing the quality of the drift process (comparable to an dispersion for electrical signals on a transmission line) depending inversely on E while the minimum is governed by the relation kT/E, the thermal limit. If measurements are found above this limit, the electrons are not in equilibrium with the gas. The cooling effect of the molecular gases is clearly seen. The goal of the choice of gas in a drift chamber must be to optimize this cooling which is not always evident since other practical considerations besides the drift velocity have to be taken into account: specific energy loss, photon absorption cross section, Townsend coefficient (for gas gain), magnetic deflection, electron attachment, safety regulations etc.

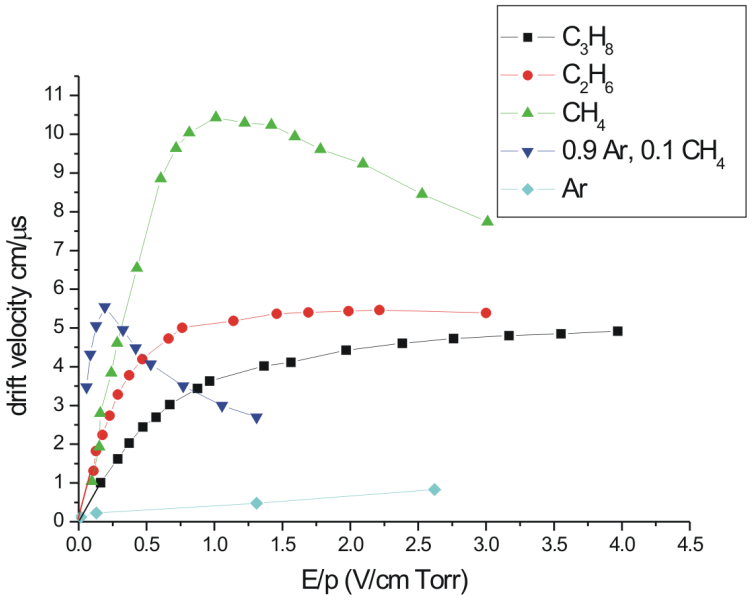

FIG. 9: *Drift velocity vs. reduced field for several gases* (CH4, C2H6, C3H8: [10] , Ar, Ar/CH4: [11])

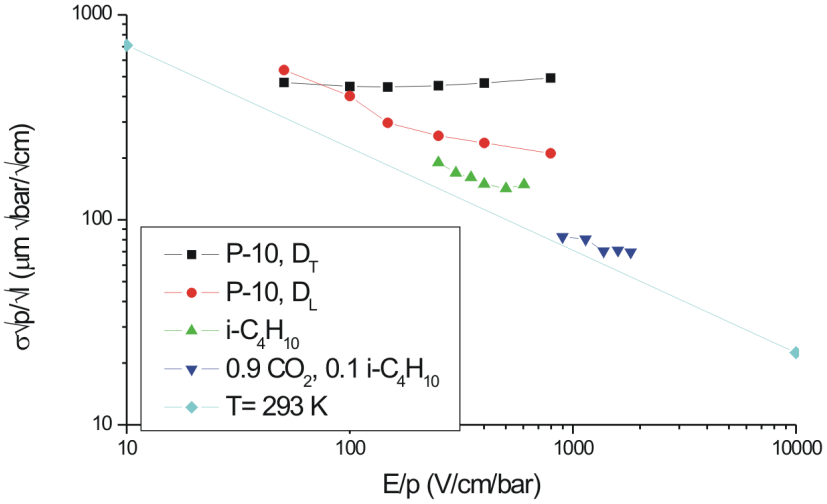

FIG. 10: *Diffusion (reduced) vs. reduced electric field for several gases* [11]

Experimental Set-up

An artist view of the setup is shown in fig. 11 displaying the main features of operation: the single sided, single cell drift chamber is moved via a sliding table through a fixed collimated beam of fast electrons (β-rays from the source, either Sr-90 or Ru-106, see fig. 12 for the decay schemes). The time of the particle passage is recorded by the signal from the photomultiplier coupled to the scintillator and the drift time is obtained from the amplified signal of the drift chamber. This time lag is measured for different positions of the drift chamber.

A schematical view of the drift chamber is shown in fig. 13 indicating the drift electrodes connected to a resistive

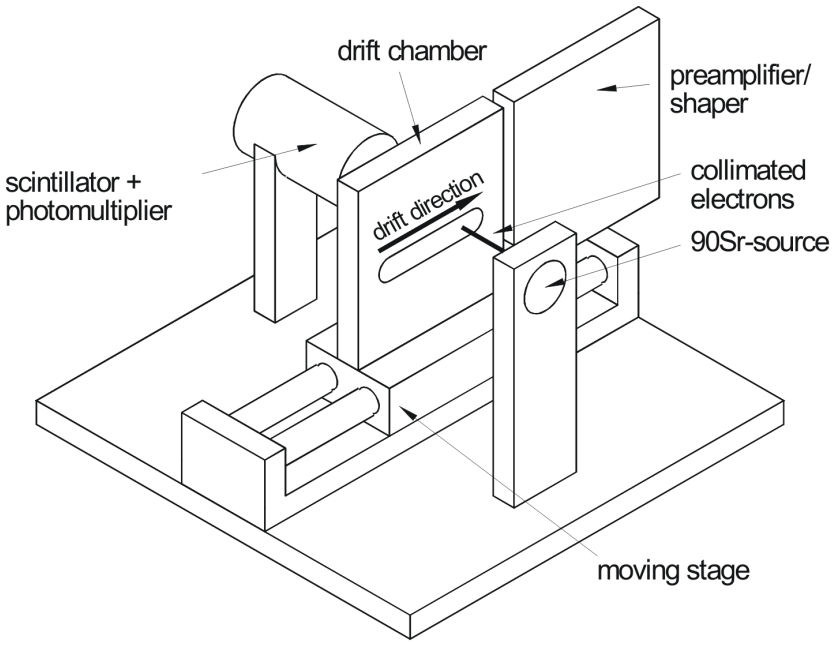

FIG. 11: *Set-up of drift chamber and source collimation*

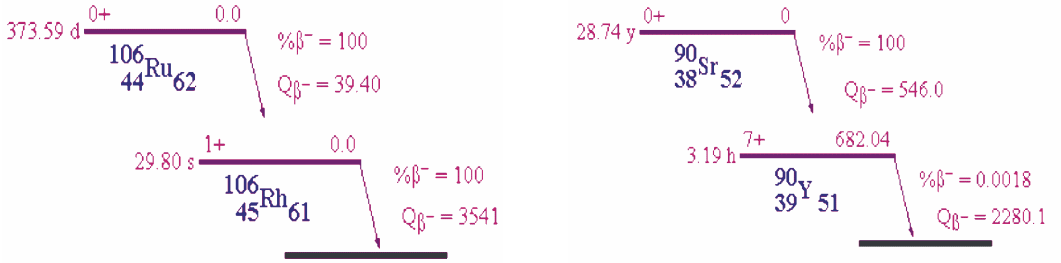

FIG. 12: *Decay schemes of radioactive sources for high-energy β-rays*

divider chain producing a constant drift field. The electrons are amplified at three anode wires of which the two outer ones are connected together. The side view (fig. 14) shows some construction details: the drift electrodes are fabricated in hybrid (thick film) technology with structured conducting electrodes (silver-palladium) and resistors deposited in a baking process on ceramic ($Al_2\ O_3$) substrate. In principle the ceramic is thin enough to allow x-rays to penetrate. In order perform measurements with minimum ionizing β -rays a slot at half height is cut into the ceramic. The electrodes are bridged by wires soldered to the conducting strips on both sides.

The amplifying structure at the end of the drift cage consists of three anode wires enclosed by 4 potential wires in order to generate a controlled transition from the drift field to the almost cylindrical amplification field around the anode wires (fig. 15) The operation of the drift chamber is controlled by two independent power supplies: one for the drift field (negative) and one for the gas gain (positive).

The preamplifier and shaper (fig. 16) of the anode signal is optimized for low noise and a shaping allowing at the same time to record the phase of the signal (drift time) with good precision and the shape due to broadening from diffusion. This is achieved by an integrating input stage and the following pole-zero cancellation. A second pole-zero cancellation removes the tails from the signal generation process in the proportional gas gain. Two more integration time constants (not shown) define an approximately gaussian width of the output pulse of approximately 150 ns. The shaped signals are recorded in a digital storage oscilloscope with respect to the trigger from the photomultiplier signal. The averaging mode of the scope allows the recording of fluctuating individual signals from the detector with good precision.

For the timing precision of the trigger signal from the scintillator-photomultiplier combination a value of about 1 ns may be easily reached, good enough for the drift time measurement. But the trigger signal also defines a spatial

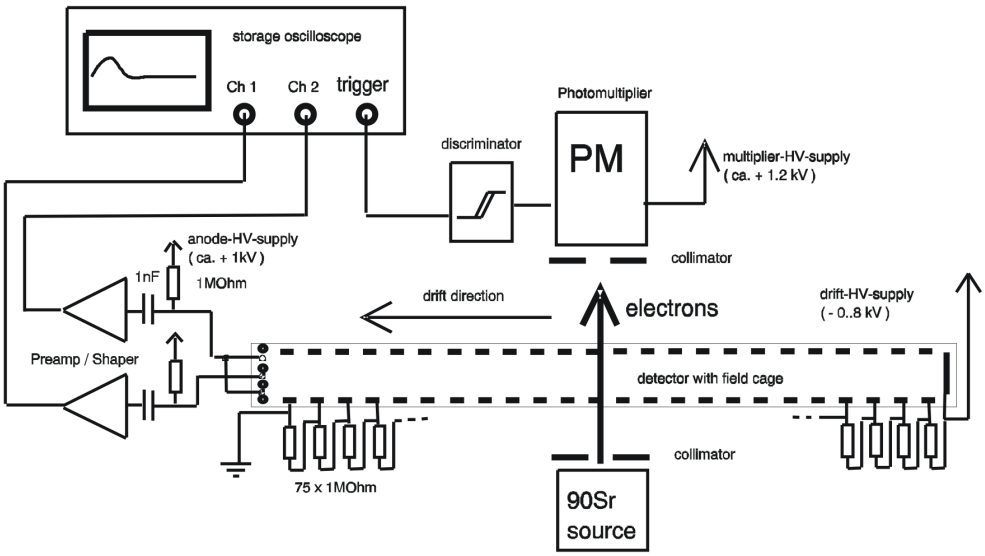

FIG. 13: *Functional set-up of experiment with drift chamber and electronics. Gas supply and HV-supplies are not shown*

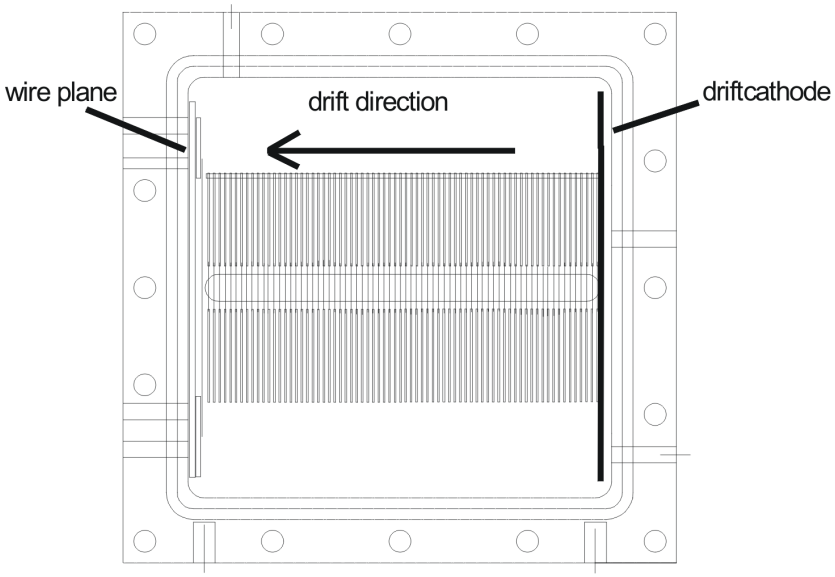

FIG. 14: *Side view of drift chamber*

selection of an ionizing particle crossing the drift space at a well-defined location. This is achieved by collimators placed at the source and the entrance of the scintillator. Beyond the geometrical limitation also bremsstrahlung and multiple scattering broaden the accepted beam. Therefore the chamber thickness has been minimized and the collimator consists of low Z material (Lucite).

The gas supply consists of a gas mixing system (fig. 17) where up to three gases supplied from pressurized bottles are mixed and distributed to all detectors at the same time. The gas mixture is defined by needle valves in the individual gas supply and controlled by calibrated flow meters. The gases are argon (a welding quality is sufficient), methane and camping gas (mostly propane and butane).

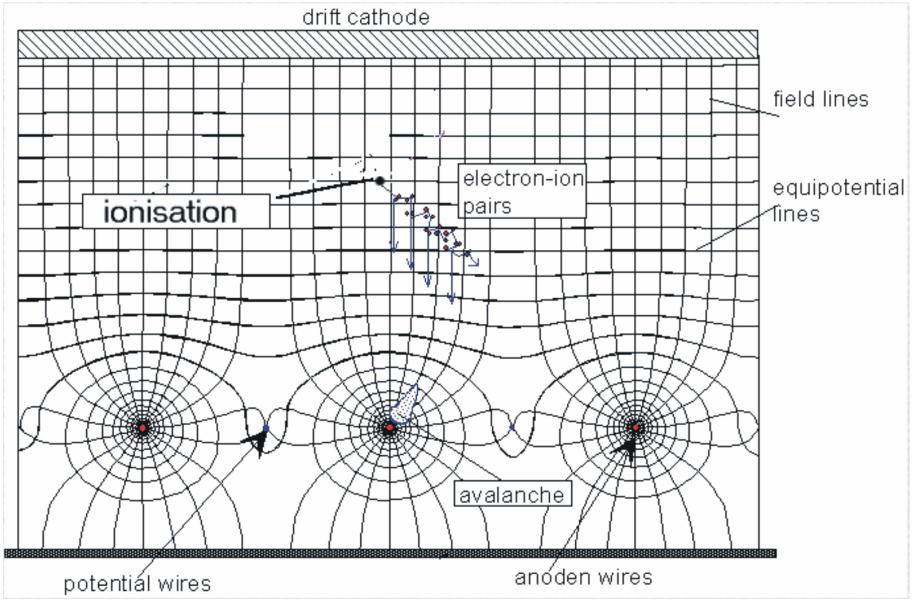

FIG. 15: *Electric field near anodes. The distance to drift cathode is not to scale*

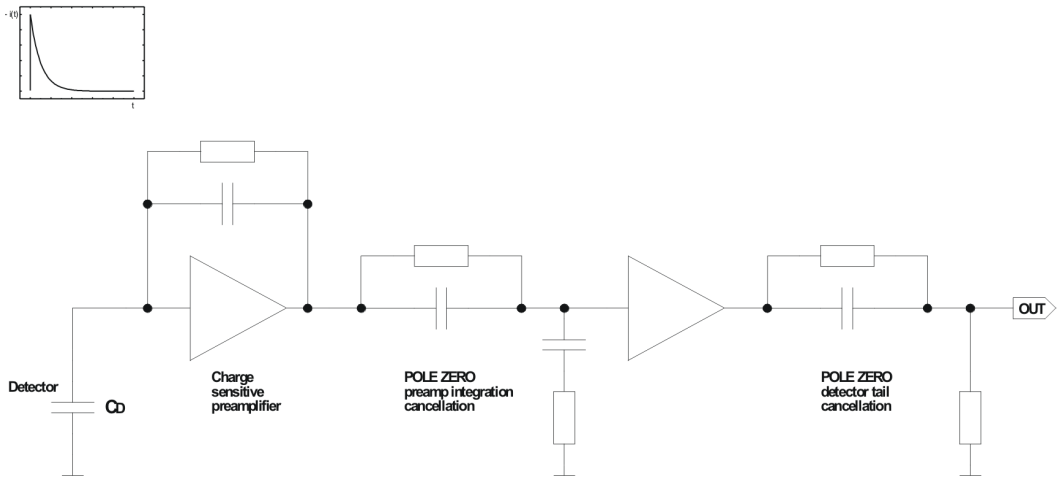

FIG. 16: *Preamplifier schematics*

Measurements

1. Preparation of the detector

After regulation of the gas flow allow about 5 minutes for full exchange of the gas in the detector. Control the flow at the outlet of the chamber. Check the operation of the amplifier by observing the noise in the single shot mode of the scope or using an analogue scope. Observe the photomultiplier signals on the scope and adjust the voltage such that in the mean a few 100 mV are obtained. Control the output of the discriminator and adjust the threshold.

2. Gas gain

For a medium setting of the drift field (ca. 2 kV) the anode voltage is increased until signals appear occasionally. For each gas mixture **a maximum allowable voltage** is given (by the assistant) which never should be exceeded, otherwise the detector will be destroyed. If this voltage is reached without observing signals, check the system again. In the averaging mode the proper signal height is adjusted by fine-tuning the gain voltage.

3. Drift velocity

The drift time is recorded at an appropriate number of detector positions. In principle a straight line should be

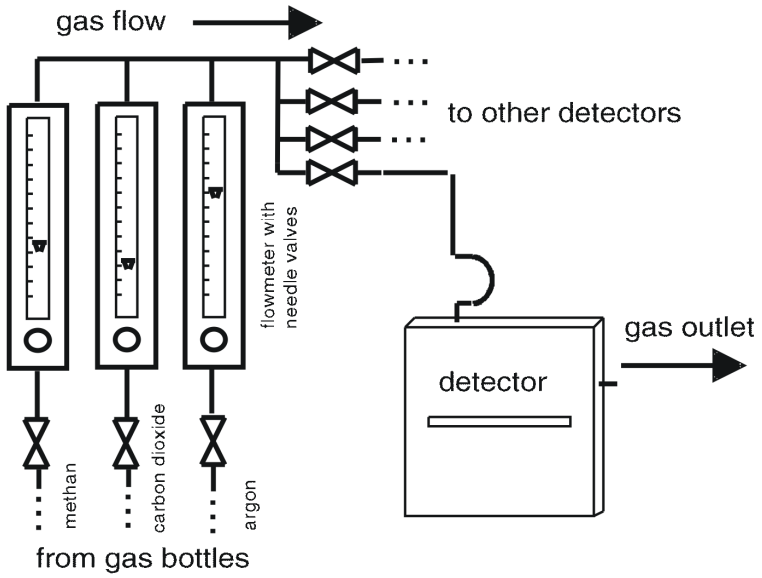

FIG. 17: *Gas mixing system*

obtained for measurements not too close to the anode. This measurement is repeated for a number of drift voltage settings and gas mixtures. It is important to control each time the gas gain (see above).

4. Diffusion

For a low drift field and small drift velocity (ca. 1 cm/μs in P-10) the signals are averaged and recorded at different positions. Although the amplitude decreases the broadening of the width at half maximum is well visible. Even if the single signal seems to disappear in the noise the averaging will sum up the signals linearly but the noise only by the square root law such that the signals finally will emerge from the noise.

Discussion of Results

The data recorded with the digital storage scope can be transferred to PCs with a mathematical and plotting program (e.g. ORIGIN).

The plots drift time vs. position allow the determination of the drift velocity at the given drift field. The measured points near the anode (distorted drift field) should be neglected. The determination of the reduced field strength E/p results in values to be compared to literature.

The plots of drift velocity vs. E/p for different gas mixtures allow the discussion of the mean electron energy and the cross sections for elastic encounters (Ramsauer effect) and inelastic encounters (rotational and excitational levels in molecules).

The plot of the width Δt of the signals vs. the position l should follow the general expression:

$$(\Delta t)^2 = a + b \cdot l \tag{16}$$

A fit to the data allows the determination of a and b. The first coefficient contains the collimation and the inherent width of the shaper while the second contains the diffusion constant D. Using equ. (14) and (15) D and T_e should be calculated and compared to the literature value of fig. 10. Possible deviations should be discussed.

The final discussion of the resolution of drift chambers may include the following effects:

- primary ionization and fluctuations
- diffusion
- signal generation

- electronic time measurement
- systematic errors and calibration

Acknowledgments

We are much grateful for the financial support of BMBF (Federal Ministry of Education and Research, Germany) and TÜBİTAK (The Scientific and Technical Research Council of Turkey) which made our participation to the school possible. We are thankful to Dipl.Phys. Dieter Gebauer from our hybrid laboratory for his work in the production of this drift chamber and in the mechanical design, to Dr. Carsten Strietzel who worked in designing this set-up and built the first set-ups which were used at previous ICFA schools and to the mechanical workshop of the physics department in Siegen for their excellent work in the mechanical set-up.

---

[1] Huxley, L. G. H., and Crompton, R. W., *The Diffusion and Drift of Electrons in Gases*, John Wiley & Sons, 0-471-42590-7.
[2] Grupen, C., *Particle Detectors*, Cambridge Monographs on Particle Physics, Nuclear Physics and Cosmology, 1996.
[3] Knoll, G. F., *Radiation Detection and Measurement*, Wiley, New York, 1989.
[4] Blum, W., and Rolandi, L., *Particle Detection with Drift Chambers*, Springer-Verlag, 1993.
[5] Walenta, A. H., *Review of Physics and Technology of Charged Particle Detectors*, Proceedings of SLAC Summer Institute on Particle Physics: Dynamics and Spectroscopy at High Energy, SLAC-R-267, 1983.
[6] Sauli, F., *Principles of Operation of Multiwire Proportional and Drift Chambers*, CERN 77-09, also in Experimental Techniques in High Energy Physics, edited by T. Ferber, Addision-Wesley, 1987.
[7] Ermilova, V. K., Kotenko L.P., Merzan G. J., and Chechin, V. A., *Ternary Specific Ionization of Relativistic Particles in Gases*, Sov. Phy. JETP, 29, 861, 1969.
[8] Fehlmann, J., and Viertel G., *Compilation of Data for Drift Chamber Operation*, ETH Zurich IHP Detector Group, August 1983.
[9] Lehnert H., *Bestimmung des Townsendkoeffizienten von Isobutan*, Diploma Thesis, University of Siegen, 1993.
[10] T.L. Cottrell and I.C. Walker, Trans. Faraday Soc., 61 (65) 1585.
[11] Mattern D., *Bestimmung des Einflusses von Driftparametern auf die Signalform einer TEC(Time Expansion Chamber)*, PhD Thesis, University of Siegen, 1988.